Structure and magnetic order of EuB_6

S. Süllow, I. Prasad, and M. C. Aronson
Department of Physics, 2071 Randall Laboratory, University of Michigan, Ann Arbor, Michigan 48109-1120

J. L. Sarrao* and Z. Fisk
National High Magnetic Field Laboratory, 1800 E. Paul Dirac Drive, Florida State University, Tallahassee, Florida 32310

D. Hristova, A. H. Lacerda, and M. F. Hundley
Los Alamos National Laboratory, Los Alamos, New Mexico 87545

A. Vigliante and D. Gibbs
Brookhaven National Laboratory, Upton, New York 11973-5000

(Received 8 September 1997; revised manuscript received 12 November 1997)

We present a study of the structural and magnetic properties of single-crystalline EuB_6. Temperature-dependent x-ray diffraction found no significant anomalies at the onset of ferromagnetic order. The resistivity, dc susceptibility, magnetization, and specific heat prove the crystal to be of extraordinarily high quality. Two ferromagnetic transitions at $T_{c1}=15.3$ K and $T_{c2}=12.5$ K are observed in all investigated properties. The ordered state displays an unexpected anisotropy, and we derive the magnetic phase diagrams for the three principal cubic directions. We argue that the two magnetic phases are connected by spin reorientation, enabled by a reduction of the crystalline symmetry from cubic. An additional anomaly in the specific heat is observed at low temperatures, which we interpret as arising from the splitting of the Eu ground-state multiplet in internal magnetic fields. [S0163-1829(98)00610-9]

I. INTRODUCTION

Hexaboride compounds RB_6 (R=rare earth or alkaline metals) are one of the most intensively studied groups of intermetallic compounds. They crystallize in a simple cubic lattice (space group 221, $Pm3m$; CaB_6 type) and exhibit a large variety of physical ground states (for a review see Ref. 1). Simple band metals (LaB_6) are found as well as conventional local moment magnets (GdB_6) or dense Kondo systems (CeB_6). This richness of phenomena combined with crystallographic simplicity makes the hexaborides ideal model systems for studying the electronic and magnetic properties of intermetallics.

The rare-earth hexaborides have been investigated in detail, and many of them are well understood. Notable exceptions are EuB_6 and SmB_6. While Sm_6 is a valence-fluctuating Kondo gap material,[2] the previously established view of divalent EuB_6 is as a ferromagnetic semiconductor.[3–7] This identification was prompted by the findings of tight-binding band structure calculations,[8] which predicted that all divalent hexaborides should be insulating, as two electrons completely fill the B-based valence band. However, subsequent authors argued on the basis of a positive temperature coefficient of the resistivity that EuB_6 is a semimetal rather than a semiconductor,[9] a view in agreement with the most recent self-consistent band structure calculations.[10,11]

The electronic and magnetic ground states of EuB_6 are related, but neither is firmly established. Initially, single-crystalline specimens were reported to undergo a single ferromagnetic transition at $T_c \approx 13$ K.[5,9] Later it was revealed that two magnetic transitions are present.[12,13] The appearances of the transitions in transport and thermodynamic properties raise questions about their character and the type of the underlying magnetic interaction.[9,12,14–16] It was even argued that the magnetic transitions are accompanied by a semimetal-metal transition, resembling that of collosal magnetoresistance compounds.[13]

Strong sample dependences complicate matters, making it difficult to unambiguously identify the intrinsic magnetic and transport properties of EuB_6. Small amounts of impurities drive the system into a semiconducting, antiferromagnetic ground state.[17,18] Moreover, EuB_6 can form in a wide homogeneity range [$Eu_{0.9}B_6$–$EuB_{5.93}$ (Refs. 19–21)], introducing a possible role for vacancies and strain. This subject was addressed for divalent SrB_6, where it was speculated that a minute degree of lattice distortion heavily affects its physical properties.[22]

Here we reopen the unsolved case of EuB_6. We present a study of the structural and physical bulk properties of a high-quality single-crystalline specimen. Our main interests lie with the magnetic properties of EuB_6, and in particular the symbiotic relationships among the magnetic transitions, their anisotropy, and the structural properties of EuB_6.

In Sec. II we introduce our data on the low-temperature structural properties of EuB_6, obtained in a high-resolution x-ray-diffraction experiment. Our aim was to determine if the magnetic transitions in EuB_6 are accompanied or triggered by structural anomalies. We do find a structural anomaly, though within the resolution of our experiments we cannot unambiguously relate the anomaly to a symmetry lowering and the magnetic properties of our crystal.

In Sec. III we present experiments on the physical bulk properties (resistivity ρ, susceptibility χ, magnetization M,

and specific heat c_p) of our single crystal. Two ferromagnetic transitions at $T_{c1}=15.3$ K and $T_{c2}=12.5$ K are observed in all investigated quantities. The two transitions exhibit pronounced anisotropy and are sensitive to the application of small magnetic fields.

We discuss our results in Sec. IV. The presence of two magnetic transitions indicates the near degeneracy of two ferromagnetic spin alignments. This degeneracy of two spin states explains most of the magnetic properties of EuB_6, like the soft ferromagnetism, the sample dependences of the magnetic properties, and the comparatively broad features in the specific heat at the magnetic transitions. We attribute an additional anomaly in the specific heat at even lower temperatures to crystalline electric field excitations.

II. STRUCTURAL PROPERTIES

The single-crystalline EuB_6 was prepared by solution growth from Al flux as described in Ref. 9, only here borothermal reduced EuB_6 powder was used instead of the pure elements (purity of the starting material: Eu, 99.99% in Eu_2O_3; B, 99.9%; Al, 99.999%). After dissolving the Al flux in NaOH solution a crystal of about 1.5 mg was extracted. The crystalline bar of $0.6\times0.3\times2.1$ mm and black color possesses flat, mirrorlike surfaces. X-ray diffraction proves these surfaces to be parallel to the [100] and [110] directions of the cubic unit cell.

There are severe symmetry restrictions on the possible magnetic structures for a given crystalline symmetry, and in particular, the appearance of two ferromagnetic transitions in a cubic crystal of symmetry $m3m$ is impossible.[23] To determine accurately the symmetry of our crystal we therefore executed a high-resolution x-ray-diffraction study. This was done at the X22C beam line of the National Synchrotron Light Source at Brookhaven National Laboratory using an x-ray wavelength of $\lambda=1.54983$ Å. The sample was mounted on the end of a helium displex refrigerator, allowing the temperature to be adjusted between 8 and 300 K. Some mosaicity of the crystal was found in initial experiments, indicating that the sample consists of two smaller pieces with a 0.2^o mismatch. In order to simplify the diffraction pattern and reduce the signal-to-noise ratio, the beam was centered on one of the two pieces (mosaicity $\approx0.02^o$ in all experiments presented here).

Two types of experiments were performed: (i) the temperature dependence of the lattice parameter a was measured in the range of the magnetic transitions, between 8 and 20 K and (ii) the intensity distribution of the Bragg peaks was investigated in reciprocal space.

In Fig. 1 we present the result of the first experiment, which is the temperature dependence of the lattice parameter a. Overall, the value of a is in good agreement with previously published data.[9,19–21,24] At the magnetic transitions we do not see a significant change of the lattice parameter a, thus ruling out massive structural changes accompanying the transitions. From recent pressure experiments, observing an increase of both magnetic transition temperatures, and employing Ehrenfest's relation an increase of a at the transition would be expected.[16] This change of the lattice constant, however, is too small to be detected in our study. Thermal expansion experiments are planned for the future to investigate more closely the relation between a and temperature T.

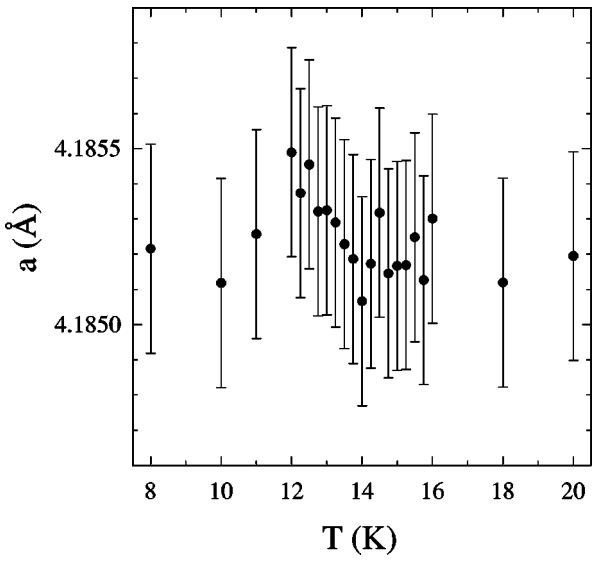

FIG. 1. The lattice parameter of the cubic unit cell a of EuB_6 as a function of temperature in the magnetic transition regime, determined from the [100] and [200] Bragg peaks.

The primary result of the second experiment is depicted in Fig. 2. We plot the measured x-ray intensity in one quadrant of $[h0l]$ space close to the [300] Bragg peak at 20 K; similar results have been found at other Bragg peaks. Remarkably, the intensity distribution of the Bragg peak is not isotropic in the hl plane. Instead, wings protrude from the side of the

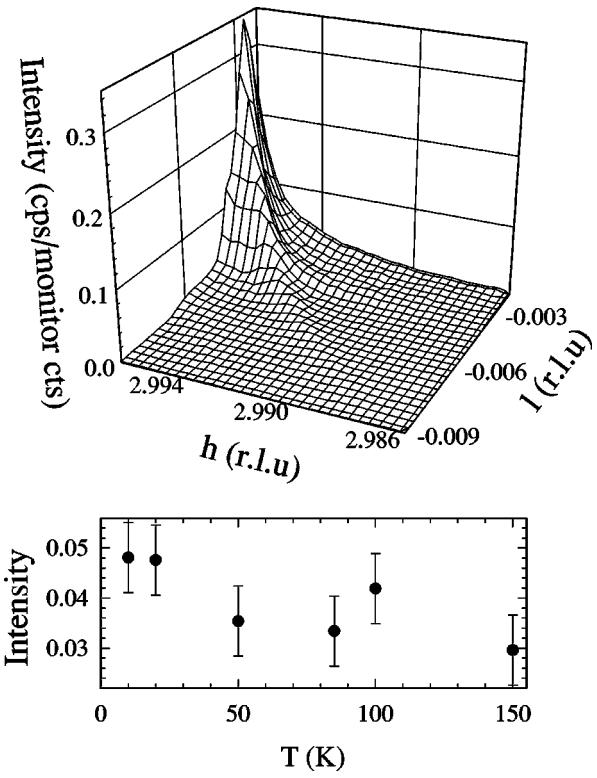

FIG. 2. Upper panel: the intensity distribution in one quadrant of reciprocal space $[h0l]$ close to the [300] Bragg peak at 20 K, exhibiting the wing extending from the side of the Bragg peak. Lower panel: the temperature dependence of the maximum intensity of the wing at $[3.01,0,4.5\times10^{-3}]$.

Bragg peak. The intensity distribution of the Bragg peaks themselves was well described by an approximately resolution-limited Lorentzian function, corresponding to a structural correlation length of $\geqslant 4000$ Å. The wings at the Bragg peaks are found in all (hl, hk, and kl) planes. In a given plane, each Bragg peak has four symmetrically arranged wings. For instance, in the $h0l$ plane the wings point along $[h0l]$, $[-h0l]$, $[h0-l]$, and $[-h0-l]$. Their intensities, however, differ slightly from wing to wing. The direction of the wings in $[hkl]$ space is not related to a high-symmetry axis of the lattice; the relative direction of the wing in Fig. 2 is $[-302]$. Also, this direction in reciprocal space varies from Bragg peak to Bragg peak; the relative direction of the wing at the [200] peak is [301]. Further, in the lower panel of Fig. 2 we plot the maximum intensity of the wing at [3.01,0,0.0045] as a function of T. While increasing the temperature from 10 to 150 K, the intensity slightly decreases. Finally, no change of the wing shape or intensity is observed while passing through the magnetic transitions.

One often cited mechanism causing such wings, thermal diffuse scattering, seems to be excluded by the temperature dependence of the wing intensity. The energy scale of thermal diffuse scattering is set by the Debye temperature Θ_D, which is 162 K for the Eu mode in EuB_6 (see the discussion of specific heat in Sec. III). If the wings arise from thermal diffuse scattering, we would expect a substantial increase of the wing's intensity as the temperature increases, since our experiment varies T from $\Theta_D/10$ to Θ_D. In contrast, we observe a small decrease of the x-ray intensity.

Several other explanations for the wings, like strain at the sample surface, lattice disorder, vacancies, or an incipent structural distortion, could be possible. Unfortunately, at present we cannot determine which of these apply to EuB_6. With respect to our initial goal to determine if a symmetry-lowering distortion appears in EuB_6, we are unable to relate any of these explanations unambiguously to such a distortion. A more sophisticated treatment and more extensive data set would be required to obtain this information on the microstructure and symmetry of EuB_6.

III. PHYSICAL PROPERTIES

We now introduce the physical bulk properties of our crystal. In Fig. 3 we display the resistivity ρ of EuB_6, measured for $I \| [100]$. Metallicity is indicated by a decreasing ρ as T decreases from 300 to 30 K. Below 30 K the resistivity increases and goes through a maximum, defining the upper magnetic transition. These data resemble those of earlier studies,[5,6,9,14,15,24] although we observe a lower residual resistivity ($\rho_{1.5\,K} = 8.7\ \mu\Omega$ cm) and a higher residual resistivity ratio ($RRR = \rho_{300\,K}/\rho_{1.5\,K} \approx 86$), indicating a high-quality crystal. To illustrate this point further and to put our results in perspective we summarize experimentally reported values for resistivity ratios, residual resistivities, and magnetic ordering temperatures in Table I. A clear correlation exists between the values of the ordering temperatures and the resistivity ratio and residual resistivity.

A cusplike anomaly at the upper and a shoulder at the lower transition mark the onset of magnetic order in the resistivity. This is illustrated in Fig. 4, where we plot the low-temperature resistivity of EuB_6. Susceptibility measurements

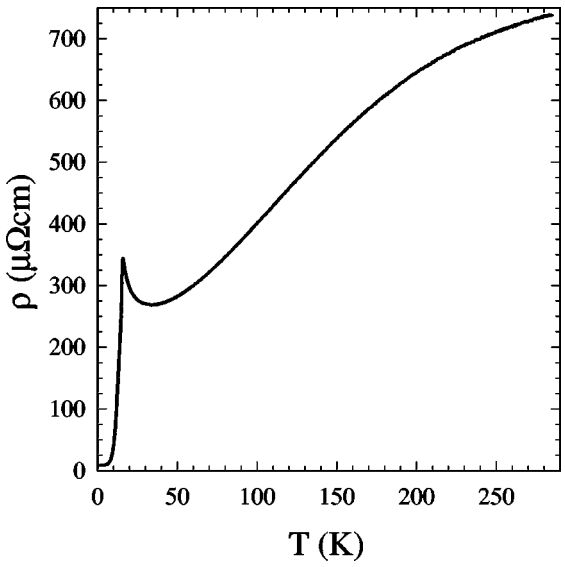

FIG. 3. The temperature dependence of the electrical resistivity of single-crystalline EuB_6 between 1.5 and 300 K.

(see below) prove both transitions to be ferromagnetic. We determine the magnetic transition temperatures from the maxima in $d\rho/dT$ as $T_{c1} = 15.3$ K and $T_{c2} = 12.7$ K.

Commonly, for ferromagnetic metals far below the magnetic transition the resistivity drops with T^2 because of electron-electron and—to a smaller degree—electron-magnon scattering.[26] In EuB_6 this is not the case. Fitting the resistivity below $T_{c1}/2$ to $\rho = \rho_0 + AT^x$ yields the unphysical result $x = 4.7$. Instead, the strong T dependence is better associated with the opening of a magnon gap as discussed by Andersen,[27]

$$\rho = \rho_0 + a\frac{T}{\Delta}\left(1 + 2\frac{T}{\Delta}\right)e^{-\Delta/T}. \tag{1}$$

This expression, which is valid at temperatures sufficiently far below T_c, has been used sucessfully to describe the resistivity in the magnetically ordered state of certain U compounds.[28–32] Below 10 K, Eq. (1) can be fit to the resistivity of EuB_6 with a magnon gap $\Delta = 45 \pm 1$ K. The result of the fit is included in Fig. 4 as a solid line.

TABLE I. Reported values of resistivity ratios $\rho/\rho_{300\,K}$, residual resistivities, and ferromagnetic transition temperatures T_{c1} and T_{c2}.

$\rho/\rho_{300\,K}$	$\rho \to T = 0$ K [$\mu\Omega$ cm]	T_{c1} [K]	T_{c2} [K]	Reference
86	8.7	15.3	12.7	[this work]
35	10	14	9	5
60	10	13.7	[a]	9
42.5	14.5	13.7	[a]	15
1	150	($T_N \approx 5$ K) [b]	[b]	18
56	20	14.5	[a]	24
40	20	12.5	[a]	25

[a]Only one ferromagnetic transition observed.

[b]Antiferromagnetic transition, induced by carbon impurities.

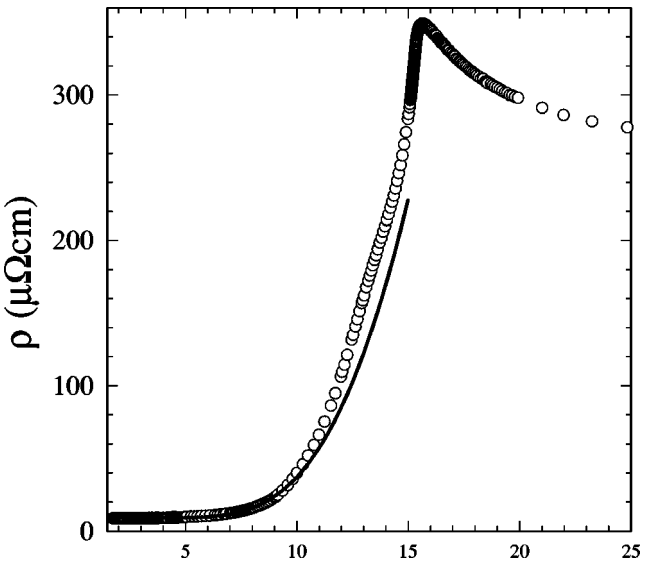

FIG. 4. The low-temperature resistivity with the magnetic transitions of EuB_6 (○). The solid line indicates a fit of the data to Eq. (1) below 10 K.

Further, as depicted in Fig. 5, a large negative magnetoresistance is observed in EuB_6 near the ferromagnetic transitions. The magnetoresistance of our sample is similar to that reported in earlier studies.[5,15]

At high temperatures, the susceptibility χ of EuB_6 follows a Curie-Weiss behavior for the three main cubic unit-cell directions (Fig. 6). Fitting χ above 50 K to Curie-Weiss functions yields the effective high-temperature moments μ_{eff}, $7.9\mu_B\|[100]$, $8.0\mu_B\|[110]$, and $8.2\mu_B\|[111]$, and Curie temperatures Θ_C, 14 K$\|$[100], 15 K$\|$[110], and 14 K$\|$[111]. The values of μ_{eff} are in good agreement with the magnetic moment of the Eu^{2+} ion calculated from Hund's rule, $7.94\mu_B$. The Curie temperatures are in accord with the observed ferromagnetic ordering at about 15 K. Finally, no indications for (crystalline electric field) anisotropy among the three cube directions in the paramagnetic phase can be found within the absolute experimental error.[33]

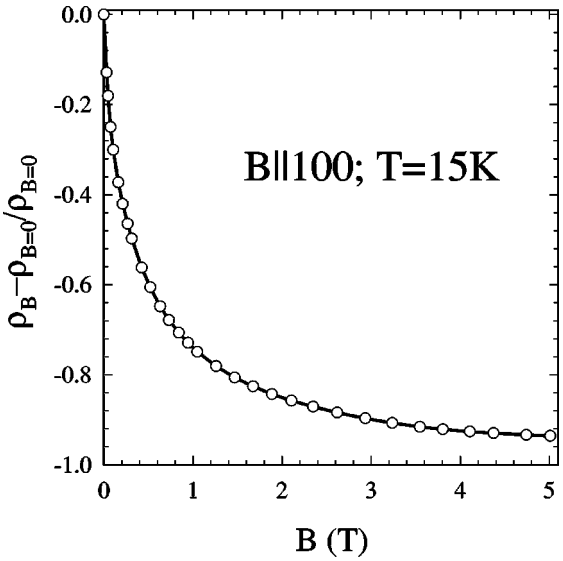

FIG. 5. The magnetoresistivity of EuB_6 measured for $B\|I\|[100]$ at 15 K (○).

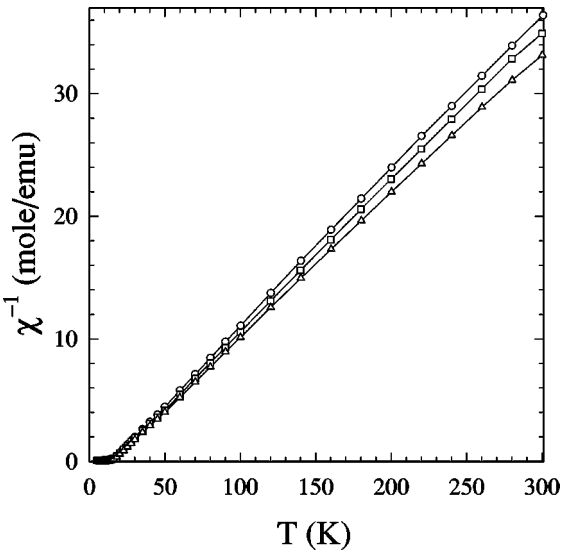

FIG. 6. The inverse magnetic susceptibility of EuB_6, measured in a field $B=0.1$ T directed along the three principal directions of the cubic unit cell: (○)$\|$[100], (□)$\|$[110], and (△)$\|$[111].

In Figs. 7(a)–7(c) we display the low-temperature susceptibility along the three cubic directions. The data are corrected for demagnetization effects. The sudden increase of χ, the kink, and the subsequent saturation mark the upper ferromagnetic transition. From the minimum of $d\chi/dT$ we find $T_{c1}=15.2$ K in 0.005 T. Expanding the saturation region of χ below T_{c1} for $B\|$[100] and [111], as is done in Fig. 8, reveals for both directions the second magnetic transition, visible as change of slope at $T_{c2}\approx 12$ K. A similar observation is made along [110]. Below the second transition the susceptibility is flat and featureless to the lowest measured temperatures (2 K) for all three directions.

Distinct magnetic anisotropy, both in absolute values and in the field dependence of χ, is present in the magnetically ordered state (Fig. 7). For $B\rightarrow 0$ T, the susceptibility along [111] in the ordered state is about 10 times larger than along [100] or [110]. This cannot be an artifact from underestimating demagnetization effects in our experiments. In the uncorrected data, the susceptibility along [111] is 6 times larger than along [100] or [110], implying that demagnetization corrections only increase the anisotropy between [111] and [100]/[110].

The anisotropy is related to the two magnetic transitions, as can be seen from the field dependence of χ for the different crystallographic directions. A small magnetic field of 0.02 T applied along [100] or [110] hardly affects the upper magnetic transition, while it easily suppresses T_{c1}, coinciding in 0.02 T with T_{c2}, if the field is applied along [111]. Increasing the field to 0.1 T leads to a suppression of the absolute value of χ in the ordered state along [111], while for $B\|$[100] and [110] only the broadening of the transitions from demagnetization effects is seen (Fig. 7).

Another way to visualize the anisotropy of the magnetic phases in EuB_6 is by plotting the magnetization M along the different crystallographic directions (Fig. 9). Again the data are corrected for demagnetization effects. For all three directions typical ferromagnetic magnetization curves are found. Further, anisotropy between [100] and [111] can be seen at all temperatures and fields. The measurements along [110]

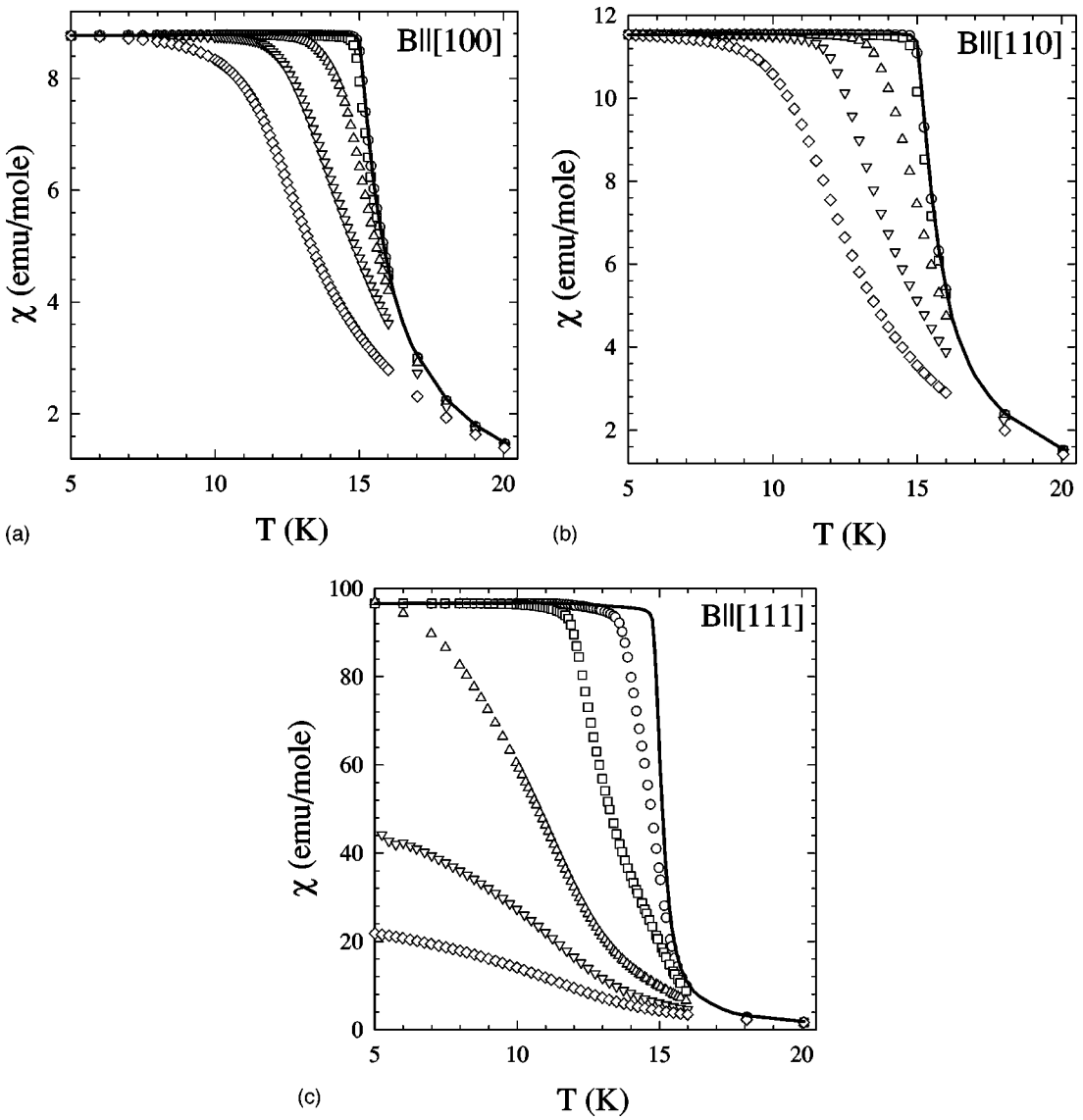

FIG. 7. The low-temperature magnetic susceptibility of EuB_6 for fields B along [100] (a), [110] (b), and [111] (c) in applied fields of 0.005 T (solid line), 0.01 T (○), 0.02 T (□), 0.05 T (△), 0.1 T (▽), and 0.2 T (◇).

lie in between: Above T_{c2} they are closer to the [100] data; below T_{c2} they follow the [111] measurements. We measured the magnetization up to 5.5 T. The magnetic moment per Eu ion approaches the value predicted from Hund's rule at the highest fields. Hysteresis loops have been measured for all three directions of the cube in the ferromagnetic state. They show EuB_6 to be a relatively soft ferromagnet compared to other localized moment magnets, as hysteresis is of the order of the experimental accuracy.

To prove that both magnetic transitions are bulk transitions, we performed a specific heat measurement, plotted in Fig. 10 as c_p/T vs T. Both magnetic transitions are evident in c_p/T, certifying their bulk character. We remark that a specific heat anomaly is seen at T_{c1}. However, the shape of the transitions is unusual. A λ-like anomaly is found for the upper transition, whose transition temperature $T_{c1}=15.1$ K is determined from the maximum in c_p. This anomaly is positioned on top of a large and broad anomaly with a plateau between 3 and 11 K. This plateau has already been seen in earlier experiments, where its considerable sample dependence was also noted.[9,12] At the lowest temperatures no temperature range can be identified in which a magnon contribution $c_p \propto T^{3/2}$, expected for simple ferromagnets, appears. We discuss the nature of the specific heat anomalies in Sec. IV.

From the Hall effect[5–7,9,15] and de Haas–van Alphen measurements[34] the number of conduction electrons in EuB_6 is found to be about 1 electron per 1000 unit cells. Then, the specific heat consists primarily of two contributions: the $4f$-electron contribution from the Eu ions and the lattice specific heat. The latter is determined from a fit of c_p above T_{c1} to the Debye and Einstein expressions for the phonon specific heat. We find $\Theta_D(\mathrm{Eu})=162$ K and $\Theta_E(\mathrm{B})=400$ K (solid line in Fig. 10). Subtracting the phonon part yields the $4f$ specific heat, from which we compute numerically the entropy of the specific heat anomaly.[35] The result of the calculation is inserted in Fig. 10. The entropy of the $4f$ specific heat saturates for $T>T_{c1}$ at about $3\ln(2)$, which is the expected value for a mole of Eu^{2+} ions.

The high quality of our crystal with respect to electronic

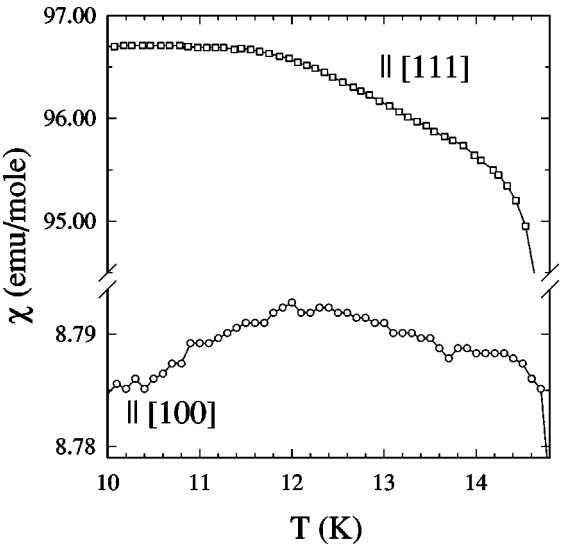

FIG. 8. The magnetic susceptibility in the ferromagnetic region below T_{c1} of EuB_6 for $B=0.005$ T, $\|[100](\bigcirc)$ and $\|[111](\square)$. The changes of slope in the ordered region indicate the second magnetic transition at T_{c2}.

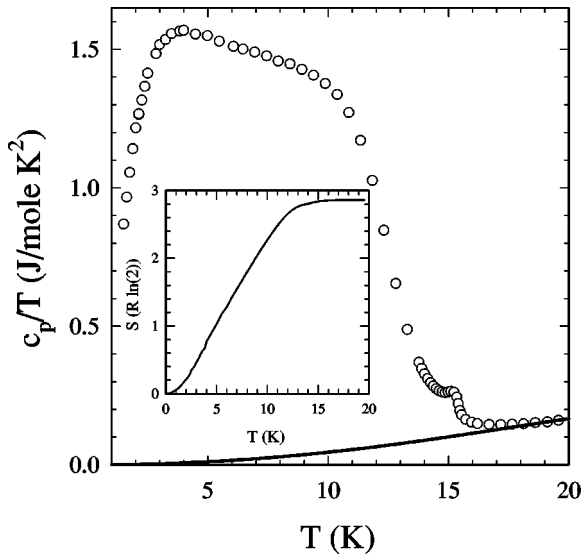

FIG. 10. The specific heat $(\bigcirc)$ of EuB_6, plotted as c_p/T vs T, in zero magnetic field, together with the lattice contribution to c_p/T (solid line). The inset shows the temperature evolution of the entropy S.

conduction is indicated by the large RRR and the low residual resistivity. The experiments on χ, M, and c_p indicate high crystalline quality with respect to its magnetic behavior. The value of T_{c1} is one of the largest reported in the literature. Susceptibility and resistivity show this transition to be an exceptionally sharp feature in temperature. Although only the specific heat anomaly below the lower transition had previously been seen, for our crystal the λ anomaly accompanying the upper transition is resolved, we believe, for the first time. While in retrospect it appears that most samples reported on in the literature show two magnetic transitions, in none of them are the two transitions as distinctive as in our crystal.

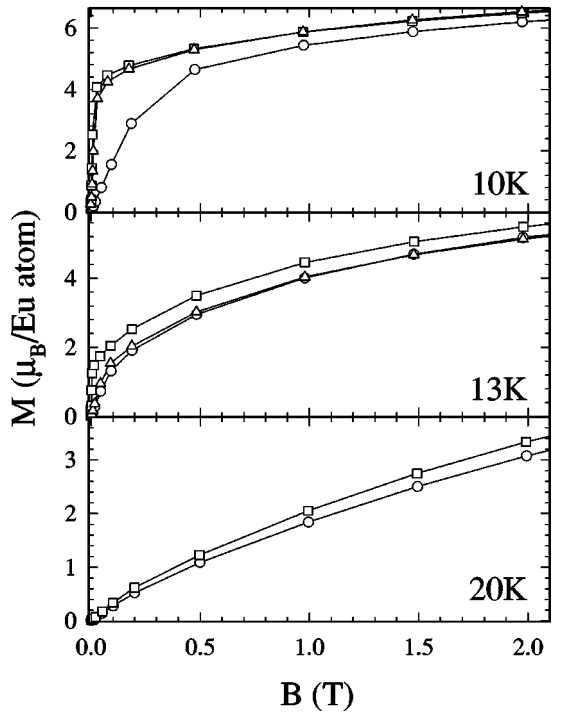

FIG. 9. The magnetization M of EuB_6 at 10, 13, and 20 K for $B\|[100](\bigcirc)$, $\|[110](\triangle)$, and $\|[111](\square)$.

IV. DISCUSSION

Our discussion must address the following points: (1) What is the magnetic ground state of EuB_6? (2) What is the origin of the double magnetic transition? (3) What is the relation between the structural and magnetic properties? The answers to these questions must account for the essential experimental facts, such as the sample dependences of physical properties, the magnetic anisotropy in the ordered state, the small ferromagnetic hysteresis, and the unusual specific heat anomaly below T_{c2}.

The large differences in the magnitude and the temperature dependences of the susceptibilities along [100]/[110] and [111] in the magnetically ordered state, as well as their different field responses, indicate that the two magnetic transitions are spin reorienations from phase I (between T_{c2} and T_{c1}) to phase II (below T_{c2}). Above T_{c1} the system is paramagnetic. These observations are summarized in the magnetic phase diagrams, which have been derived from the measurements of χ in different applied fields (Fig. 11). Transition temperatures are determined from the minimum of $d\chi/dT$ for T_{c1} and the change of slope of χ for T_{c2}. The zero-field values of T_{c1} and T_{c2} are taken from resistivity measurements.

With $B\|[100]$, the upper magnetic transition at T_{c1} is unaffected by increasing magnetic fields. Along [110], a slight decrease of T_{c1} is observed in fields up to 0.1 T. In striking contrast, if a field of 0.02 T is applied along the [111] direction, T_{c1} is suppressed below T_{c2}. Furthermore, while T_{c2} is gradually suppressed if the magnetic field is applied along [100] or [110], T_{c2} remains constant for $B\|[111]$.

These observations suggest that in zero magnetic field

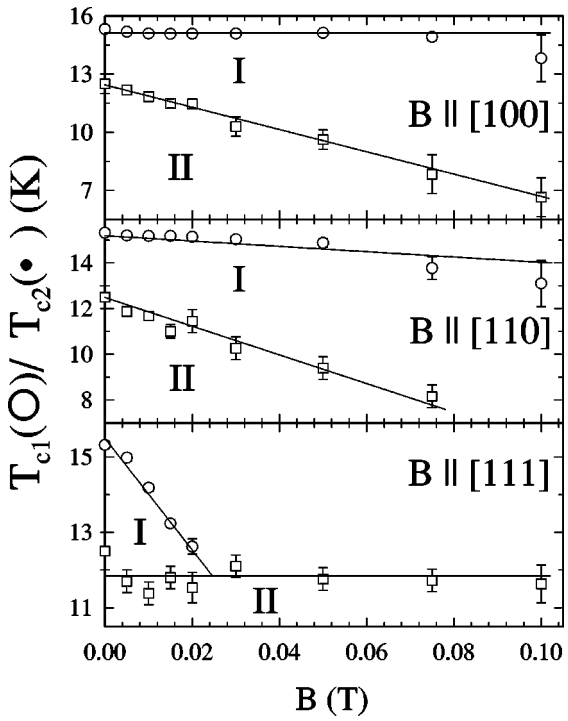

FIG. 11. The magnetic phase diagrams for the field B applied along [100], [110], and [111]. Circles (○) indicate T_{c1}, below which the magnetic phase I is found; boxes (□) delimit the magnetic phase II below T_{c2}. T_{c1} is determined as minimum of $d\chi/dT$, T_{c2} from the change of slope of χ.

[111] is the easy magnetic axis in phase II. This is consistent with χ being the largest and M having the steepest slope for B oriented along [111]. In phase I, the easy magnetic axis in zero magnetic field is along [100]. Applying a magnetic field along [100] strengthens the spin direction [100], stabilizing T_{c1} and suppressing T_{c2}. In contrast, directing a magnetic field along [111] weakens the spin alignment along [100] in phase I and suppresses T_{c1}, while it stabilizes phase II. Fields oriented along [110] mix both spin alignments and therefore have an intermediate effect on the transition temperatures. All in all, the phase diagram assigns phase II to be the magnetic ground state in small fields of any orientation. At higher temperatures phase I and paramagnetism compete. This is illustrated in Table II, where we summarize the temperature and field dependence of the different phases.

Temperature dependences of the easy magnetic direction in ferromagnets are not common in nature, but well understood in the framework of magnetic anisotropy theory. The anisotropy in a cubic crystal can be described introducing phenomenologically anisotropy parameters K_0, K_1, and K_2.[36] Spin reorientation is a consequence of the temperature dependences of K_0, K_1, and K_2. Still, it is unusual to find a temperature-dependent easy magnetic axis in a cubic Eu system. Eu^{2+} is an s-state ion with small orbital anisotropy and crystalline electric field (CEF) splitting.[37] The near cubic structure of EuB_6 suggests that it is a system with inherently small anisotropy.

TABLE II. The temperature, field and anisotropy dependence of the magnetic phases in EuB_6. In phase I the spins are aligned along [100], in phase II along [111]; P indicates the paramagnetic phase.

B [T]	$T<T_{c2}$	$T_{c2}<T<T_{c1}$	$T_{c1}<T$
0	II	I	P
$>0,\|\|[100]$	II	I	P
$>0.02,\|\|[111]$	II	P	P

The anisotropy energies can be calculated from the magnetization: $W=\int_0^{M_s} B dM$, M_s = saturation magnetization. At 4.3 K we find that the [111] direction lies about 0.28 J/cm^3 lower in energy than the [100] state [$K_0=0.43$, $K_1=-0.32$, and $K_2=-4.8$, units J/cm^3 (Ref. 36)]. At temperatures close to T_{c1} or T_{c2}, however, the calculation of the anisotropy energies becomes ambiguous. Here, the magnetization does not fully saturate up to highest fields, and the phase diagram (Fig. 11) indicates the magnetic anisotropy to be field and temperature dependent. In zero magnetic field, the phase diagram implies that close to the magnetic transitions the two spin states are energetically almost degenerated. The energy difference between the two states is of the order of $T_{c1}-T_{c2}\approx 2-3$ K. Then, some definitive experimental statements can be made.

(a) The near degeneracy of the two spin states accounts for the small hysteresis in the magnetization loops below T_{c1} or T_{c2}. A sufficiently large magnetic anisotropy is necessary for the formation of a well-defined magnetic domain state. Since EuB_6 lacks this quality, magnetic domains are easily destroyed by thermal excitations of spins from one direction into the other.

(b) The presence of two energetically similar spin states sheds some light on the sample dependences. In the structural study, we found additional structure at the Bragg peaks, possibly indicating strain or lattice disorder in our crystal of EuB_6. We assume that other crystals contain a similar structural anomaly. In ferromagnets, the crystallographic microstructure affects the magnetic anisotropy to some degree.[36] This effect is more critical than usual in EuB_6 because the delicate balance between the two spin states is determined by the difference of their anisotropy energies. A more disordered or strained sample will have a wider distribution of *local* anisotropies and anisotropy energies. This will smear out the double transition and blur related magnetic properties.

(c) Energy gaps in the magnon density of states are caused by magnetic anisotropy.[38,39] Therefore, the magnetic anisotropy in EuB_6 qualitatively accounts for the magnon gap observed in the resistivity.

(d) In group theory it is concluded that no ferromagnetic ordering can appear in $Pm3m$ symmetry. To accomodate *one* ferromagnetic structure, the symmetry of the system must be lowered to one of the tetragonal subgroups of $Pm3m$, and for *two* ferromagnetic phases the symmetry must be as low as orthorhombic.[23] In spite of this, in EuB_6 we find two magnetic phases, implying that the *true* symmetry of the system in the magnetically ordered state is lower than tetragonal.

It is a common occurrence that the experimentally observed magnetic and crystallographic symmetries of a compound are in conflict. It is generally assumed that at the phase transition the crystallographic symmetry is lowered by magnetostrictive distortion, permitting structures that would

not fit the symmetry requirements of the undistorted unit cell. For instance, small distortions are assumed to account for the low-temperature antiferromagnetism in GdB_6.[40] For antiferroquadrupolar ordered CeB_6,[41] it is assumed that a dynamic Jahn-Teller effect lowers the crystallographic symmetry.[42] For both systems the distortions are too small to be observed directly in structural investigations. A similar situation could be present in EuB_6. However, we note that it might be useful in future experiments to focus more closely on the structural anomaly observed in our x-ray study in order to determine if this anomaly affects the overall symmetry of the compound.

(e) As noted earlier[9] the specific heat at the magnetic transitions has a highly unusual temperature dependence.[43] As we will argue, this unusual behavior of the specific heat arises from a combination of contributions of the ground-state multiplet of the Eu ion and magnetic excitations in the magnetically ordered state.

As shown in Fig. 10, the $4f$ electronic entropy approaches $3\ln(2)$ just above T_{c1}. Hence, at these temperatures the full entropy of the Eu^{2+} ion has been gained and all CEF levels are fully occupied. In cubic symmetry the $^8S_{7/2}$ ground-state manifold of the Eu^{2+} is split into two doublets (Γ_6 and Γ_7) and one quartet (Γ_8). The overall splitting of these levels for the Eu^{2+} ion, which is an s-state ion, is typically of the order of some hundred mK to several K in a nonmagnetic environment.[37] We propose that the internal magnetic fields in the ferromagnetic state, amounting to several tesla at the Eu site, increase this splitting of the ground-state multiplet to about 10 K, the value necessary to produce the observed specific heat anomaly at 4 K.

Mean-field calculations lend qualitative support to our picture. Blanco *et al.*[44] calculated the specific heat anomaly of the magnetic transitions for several Gd compounds in mean-field theory. Gd^{3+}, like Eu^{2+}, is an s-state rare-earth ion with an $^8S_{7/2}$ ground-state manifold. They found that for a ferromagnetic transition the internal field splits the ground-state multiplet, which causes an anomaly in c_p at about $T_c/4$, much as we found in EuB_6.

Specific heat measurements in magnetic fields enable us to draw a schematic model for the different contributions to the specific heat of EuB_6. The observed splitting of the order of 10 K indicates that the internal fields are several tesla. We expect that external fields of comparable magnitude would lead to a substantial increase in the splitting. This effect is distinct from the demagnetization effects and modifications of the magnetic excitation spectrum, which are expected to smear out the specific heat anomalies at T_{c1} and T_{c2}.

The effects of large fields on c_p are demonstrated in Fig. 12. Note that a different crystal was used for these measurements. Since this crystal has a smaller RRR, less pronounced anomalies at the magnetic transitions, and no λ anomaly at the upper transition, we conclude that it is of lower quality than the crystal studied in the bulk of this paper. Still, the specific heat for this crystal shows the broad maximum between 3 and 10 K in zero magnetic field, similar to the result for the high-quality crystal in Fig. 10. Only some quantitative differences between the two data sets at the low-temperature anomaly can be seen, illustrating the sample dependence of c_p in EuB_6. However, for a qualitative discussion of c_p the measurements on the lower quality crystal in Fig. 12 are sufficient.

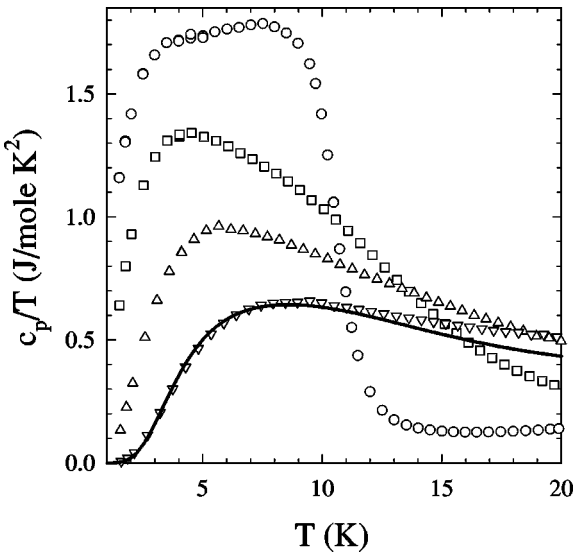

FIG. 12. The field dependence of the specific heat of EuB_6, measured for a crystal showing no anomaly at T_{c1}. The applied fields are 0 T (○), 2 T (□), 5 T (△), and 10 T (▽). The solid line results from a calculation described in the text. The lattice contribution to c_p has not been subtracted.

Applying fields up to 10 T along the [100] direction shifts the position of the low-T anomaly in c_p/T from 3 to 8–9 K. This implies that the overall splitting of the ground-state multiplet increases by the same factor and confirms our estimate of the internal fields to be of the order of 5–10 T. The zero-field anomaly at $T_{c2}=10$ K is completely destroyed in 2 T, as expected from the magnetic nature of this feature.

These measurements give a schematic picture of the different contributions to c_p. To start, we note that in 10 T the magnetic part of the specific heat is smeared out over a broad temperature range, implying that the measured specific heat below 20 K arises mostly from the ground-state multiplet and lattice contributions. To obtain a value for the order of magnitude of the splitting, we fitted the 10 T c_p data below 10 K, taking into account the lattice specific heat of EuB_6 (Sec. III). For the sake of simplicity, we took two Schottky functions, a doublet at 20 K and a quartet at 48 K, thus simulating the multiplet splitting by a CEF splitting. This oversimplifies the situation by ignoring the lifting of the level degeneracy, but it is sufficient within the limits of our schematic picture. The result of our calculation is included in Fig. 12 as solid line and is in good agreement with our data. If we now return to the zero-field measurement of c_p for the high-quality crystal (Fig. 10), we can apply our estimate of the splitting to separate the different contributions to c_p. We assume that in zero field the three specific heat anomalies are related to three different and separable effects: the anomaly at 15 K to the first magnetic transition, the upturn of the specific heat at 10 K to the ferromagnetic spin reorientation, and the downturn below 4 K to the depopulation of multiplet levels. In zero magnetic field the overall multiplet splitting must be about 2–3 times smaller than in 10 T. Thus, subtracting a Schottky contribution for a doublet at 8 K and a quartet at 20 K from the experimental data in zero field provides the temperature evolution of the magnetic part of the

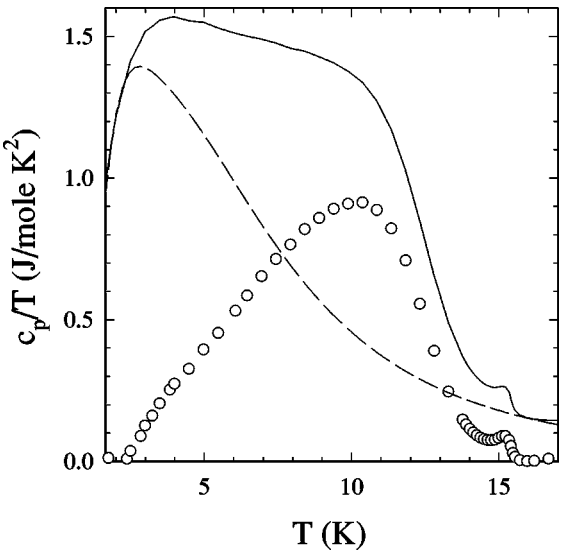

FIG. 13. The separable contributions to the zero-field specific heat of EuB_6, plotted as c_p/T vs T. The solid line denotes the total measured c_p/T, the dashed line the Schottky contribution of a doublet at 8 K and a quartet at 20 K. The magnetic specific heat c_{mag} (○) has been calculated as the difference between the total specific heat and the Schottky part.

specific heat, c_{mag}, which is plotted in Fig. 13.

Distinct maxima in c_{mag} can be seen for both magnetic transitions. The shapes of the magnetic transitions are much more in line with the expected appearances of λ anomalies, though they still look comparatively broad. Qualitatively this can be linked to the small anisotropy between the [100] and [111] states, which implies that below T_{c1} there is a low-energy excitation for the spins. Each excitation from the ground into the excited state ([111]→[100] or vice versa) disturbs the spin alignment and limits the magnetic coherence length in both magnetic phases. This leads to a broadening of the magnetic transitions in the specific heat.

In conclusion, the picture that emerges regarding the magnetic properties of EuB_6 from these experiments can be summarized as follows: The two magnetic transitions in EuB_6 are two ferromagnetic phases with different easy magnetic axes. In zero magnetic field above T_{c1} the compound is paramagnetic; between T_{c1} and T_{c2} the spins are aligned along the [100] direction, below T_{c2} along [111]. The magnetic phase diagram implies that the two states are nearly degenerate in their anisotropy energy. This explains the lack of hysteresis in the ferromagnetic state. We present evidence for a splitting of the Eu ground-state multiplet, driven by internal magnetic fields. We can qualitatively explain the unusual temperature and field dependence of the specific heat, as well as the sample dependences of the physical properties and the ferromagnetic transitions in (nominally) cubic EuB_6.

Finally, we comment on one feature of the magnetism in EuB_6. In our picture the small difference in anisotropy energy between the [100] and [111] directions in the magnetically ordered state suppresses the magnetic domain formation and limits the coherence length of the ordered state through thermally excited spin flips. Though we lack neutron-diffraction data to directly determine the magnetic coherence length, there is a way to roughly estimate the actual coherence length ξ in the magnetically ordered state. It is reasonable to assume a typical domain size for a ferromagnet of the order of 1 μm as an upper limit for ξ. Further, a lower limit for ξ can be estimated from the specific heat. Though both magnetic transitions appear broader than archetypical mean-field transitions [see, for instance, EuS (Ref. 45)], they are certainly not short-range-order transitions. This would imply a lower limit for ξ of the order of 10^3 Å. In other words, the value of ξ will be a fraction of 1 μm.

With this, EuB_6 takes an interesting position with respect to its electronic properties. In typical rare-earth magnets the electronic mean free path is much smaller than the magnetic coherence length. This is not true anymore for EuB_6; from the resistivity and measurements of the electron density (see Fisk *et al.*[9]) the low-temperature electronic mean free path l can be estimated to be of the order of 10 000 Å, thus of a similar order of magnitude as ξ. In the future it might be interesting to address this feature in more detail, in particular with respect to the unique transport properties of EuB_6.

ACKNOWLEDGMENTS

We would like to thank G. J. Nieuwenhuys for supplying us with several of his fitting programs and useful advice, R. Clarke, P. Wochner, and R. A. Robinson for fruitful discussions, and E. Tabak for assistance with the measurements. Work at the University of Michigan was supported by the U.S. Department of Energy, Office of Basic Energy Sciences, under Grant No. 94-ER-45526. Work at Los Alamos was performed under the auspices of the U.S. Department of Energy. Two of the authors, J.L.S. and Z.F., acknowledge partial support from the Japanese New Energy and Industrial Development Organization (NEDO). Work performed at Brookhaven is supported by the Division of Materials Sciences, U.S. Department of Energy under Contract No. DE AC0276CH00016.

*Present address: Los Alamos National Laboratory, Los Alamos, NM 87545.

[1] J. Etourneau and P. Hagenmuller, Philos. Mag. B **52**, 589 (1985).
[2] J. C. Nickerson, R. M. White, K. N. Lee, R. Bachmann, T. H. Geballe, and G. W. Hull, Phys. Rev. B **3**, 2030 (1971); J. C. Cooley, M. C. Aronson, Z. Fisk, and P. C. Canfield, Phys. Rev. Lett. **74**, 1629 (1995).
[3] Y. Takakuwa, S. Suzuki, and T. Sagawa, Jpn. J. Appl. Phys. **17**, 284 (1978).
[4] J. Clack, J. W. Allen, J. L. Sarrao, and Z. Fisk (private communication).
[5] T. Kasuya, K. Takegahara, M. Kasaya, Y. Isikawa, and T. Fujita, J. Phys. Colloq. **41**, C5-161 (1980).
[6] J. M. Tarascon, J. Etourneau, P. Dordor, P. Hagenmuller, M. Kasaya, and J. M. D. Coey, J. Appl. Phys. **51**, 574 (1980).
[7] S. von Molnar, J. M. Tarascon, and J. Etourneau, J. Appl. Phys. **52**, 2158 (1981).
[8] H. C. Longuet-Higgins and M. de V. Roberts, Proc. R. Soc. London, Ser. A **224**, 337 (1954).
[9] Z. Fisk, D. C. Johnston, B. Cornut, S. von Molnar, S. Oseroff, and R. Calvo, J. Appl. Phys. **50**, 1911 (1979).
[10] A. Hasegawa and A. Yanase, J. Phys. C **12**, 5431 (1979).

[11] S. Massidda, A. Continenza, T. M. de Pascale, and R. Monnier, Z. Phys. B **102**, 83 (1997).
[12] T. Fujita, M. Suzuki, and Y. Isikawa, Solid State Commun. **33**, 947 (1980).
[13] L. Degiorgi, E. Felder, H. R. Ott, J. L. Sarrao, and Z. Fisk, Phys. Rev. Lett. **79**, 5134 (1997).
[14] R. Bachmann, K. Lee, T. H. Geballe, and A. Menth, J. Appl. Phys. **41**, 1431 (1970).
[15] C. N. Guy, S. von Molnar, J. Etourneau, and Z. Fisk, Solid State Commun. **33**, 1055 (1980).
[16] J. C. Cooley, M. C. Aronson, J. L. Sarrao, and Z. Fisk, Phys. Rev. B **56**, 14 541 (1997).
[17] T. Tanaka, E. Bannai, S. Kawai, Y. Isikawa, and M. Kasaya, J. Cryst. Growth **40**, 125 (1977).
[18] Y. Isikawa, M. M. Bajaj, M. Kasaya, T. Tanaka, and E. Bannai, Solid State Commun. **22**, 573 (1977).
[19] K. Schwetz and A. Lipp, J. Less-Common Met. **33**, 295 (1973).
[20] V. N. Gurin, M. M. Korsukova, S. P. Nikanorov, I. A. Smirnov, N. N. Stepanov, and S. G. Shul'man, J. Less-Common Met. **67**, 115 (1979).
[21] M. K. Blomberg, M. J. Merisalo, M. M. Korsukova, and V. N. Gurin, J. Alloys Compd. **217**, 123 (1995).
[22] H. R. Ott, M. Chernikov, E. Felder, L. Degiorgi, E. G. Moshopoulou, J. L. Sarrao, and Z. Fisk, Z. Phys. B **102**, 337 (1997).
[23] W. Opechowski and R. Guccione, in *Magnetism*, edited by G. T. Rado and H. Suhl (Academic Press, New York, 1965), Vol. IIa, p. 105.
[24] G. Weill, I. A. Smirnov, and V. N. Gurin, J. Phys. Colloq. **41**, C5-185 (1980).
[25] M. Kasaya, J. M. Tarascon, J. Etourneau, and P. Hagenmuller, Mater. Res. Bull. **13**, 751 (1978).
[26] I. A. Campbell and A. Fert, in *Ferromagnetic Materials*, edited by E. P. Wohlfarth (North-Holland, Amsterdam, 1982), Vol. 3, p. 747.
[27] N. H. Andersen, in *Crystalline Electric Field and Structural Effects in f-electron systems*, edited by J. E. Crow, R. P. Guertin, and T. W. Mihalisin (Plenum, New York, 1980), p. 373.
[28] T. T. M. Palstra, A. A. Menovsky, and J. A. Mydosh, Phys. Rev. B **33**, 6527 (1986); S. A. M. Mentink, T. E. Mason, S. Süllow, G. J. Nieuwenhuys, A. A. Menovsky, J. A. Mydosh, and J. A. A. J. Perenboom, *ibid.* **53**, R6014 (1996).
[29] Y. Dalichaouch, M. C. de Andrade, and M. B. Maple, Phys. Rev. B **46**, 8671 (1992).
[30] K. Bakker, A. de Visser, L. T. Tai, A. A. Menovsky, and J. J. M. Franse, Solid State Commun. **86**, 487 (1993).
[31] M. Huth, A. Kaldowski, J. Hessert, T. Steinborn, and H. Adrian, Solid State Commun. **87**, 1133 (1993).
[32] B. Becker, S. Ramakrishnan, A. A. Menovsky, G. J. Nieuwenhuys, and J. A. Mydosh, Phys. Rev. Lett. **78**, 1347 (1997).
[33] The susceptibility measurements have been performed in a commercial superconducting quantum interference device (SQUID). The absolute error for our sample is determined by the sample holder contribution (about 10% of the absolute measured signal at room temperatures) and irreproducibilities in the positioning of the sample in the SQUID pickup coils.
[34] From de Haas–van Alphen measurements for the particular sample investigated in this work the electron density is found to be 0.001 electrons per unit cell; M.C. Aronson, J.L. Sarrao, Z. Fisk, and B. Brandt (unpublished).
[35] From the low-temperature specific heat a linear extrapolation to $T \rightarrow 0$ K was performed to compute the entropy below 1.4 K, which contributes less than 4% to the total entropy.
[36] E. A. Turov, *Physical Properties of Magnetically Ordered Crystals* (Academic Press, New York, 1965); F. Brailsford, *Physical Principles of Magnetism* (D. van Nostrand Company Ltd., London, 1966); R. M. Bozorth, *Ferromagnetism* (IEEE Press, Piscataway, 1993).
[37] A. Abragam and B. Bleaney, *Electron Paramagnetic Resonance Of Transition Ions* (Dover Publications Inc., New York, 1986).
[38] A. Schröder, H. von Löhneysen, and W. Bauhofer, Phys. Rev. Lett. **57**, 622 (1986).
[39] B. Coqblin, *The Electronic Structure of Rare-Earth Metals and Alloys* (Academic Press, London, 1977).
[40] H. Nozaki, T. Tanaka, and Y. Izhizawa, J. Phys. C **13**, 2751 (1980).
[41] J. M. Effantin, J. Rossat-Mignod, P. Burlet, H. Bartholin, S. Kunii, and T. Kasuya, J. Magn. Magn. Mater. **47&48**, 145 (1985).
[42] E. Zirngiebl, B. Hillebrands, S. Blumenroder, G. Güntherodt, M. Loewenhaupt, J. M. Carpenter, K. Winzer, and Z. Fisk, Phys. Rev. B **30**, 4052 (1984).
[43] Such behavior has been seen more often for Eu compounds, for instance, in orthorhombic $EuNi_5P_3$; see R. A. Fisher, P. Radhakrishna, N. E. Phillips, J. V. Badding, and A. M. Stacy, Phys. Rev. B **52**, 13 519 (1995).
[44] J. A. Blanco, D. Gignoux, and D. Schmitt, Phys. Rev. B **43**, 13 145 (1991).
[45] J. Wosnitza and H. von Löhneysen, Europhys. Lett. **10**, 381 (1989).